1376 *Biochemistry* **2011,** *50,* 1376–1383
DOI: 10.1021/bi101941c

BIOCHEMISTRY
including biophysical chemistry & molecular biology
Article

E6*, the 50 Amino Acid Product of the Most Abundant Spliced Transcript of the E6 Oncoprotein in High-Risk Human Papillomavirus, Is a Promiscuous Folder and Binder†

Angeles Heer,‡ Leonardo G. Alonso,§ and Gonzalo de Prat-Gay*,‡

‡*Instituto Leloir and Instituto de Investigaciones Bioquímicas-Conicet, Patricias Argentinas 435, (1405) Buenos Aires, Argentina, and* §*XBio Inc., Concepción Arenal 4220, D150 (1427) Buenos Aires, Argentina*

Received November 16, 2010; Revised Manuscript Received January 7, 2011

ABSTRACT: High-risk human papillomavirus E6 participates in tumorigenic progression, mainly by its ability to promote p53 degradation. HPV transcripts show a complex splicing pattern, where E6* is the most abundant transcript in high-risk HPV types, comprising the first 50 amino acids of E6. No structural or biochemical information of this polypeptide, which contains half of the first zinc binding motif of E6, is available, due to the difficulty to acquire a compact monomeric fold in such a small polypeptide. We show that HPV16-E6* can fold into either α-helix or *β*-sheet large oligomers at pH 7.5 and 5.0, respectively, in the absence of zinc. The *β*-sheet oligomers are highly stable and unaffected by the presence of zinc, while the α-helix oligomers tend to rapidly form aggregates, prevented by the presence of the metal. Two E6* molecules bind per atom of zinc, suggesting a tetrahedral, high-affinity arrangement ($K_D < 10^{-12}$ M), which results in a zinc-mediated E6* dimer with significant secondary structure. Endogenous E6 oligomers were previously found in the cytosol of high-risk HPV transformed cell lines, and we propose that the oligomerization determinant resides within E6*. E6* effects were reported to counteract those of E6 in cells, and the ratio between these two species modulates p53 degradation and other apoptosis-dependent signaling cascades. A residue of an evolved splicing event related to regulation of oncogene expression in HPV or a splicing event resulting from the selection of a small deleterious viral polypeptide, the abundant existence of E6* with a "chameleon" nature correlates with target plasticity, and its fate is linked to a balance between protein levels, zinc availability, redox potential, and oligomerization. In addition, the results presented here have strong implications for zinc binding sites in nascent polypeptides. This evolved promiscuous folder speaks of effect rather than function of a viral product that, when highly increased, can directly or indirectly affect various cellular processes leading to cell deregulation and tumorigenesis.

Human papillomavirus (HPV)[1] is a small DNA tumor virus that is directly linked to cervical and several different types of cancers associated to epithelia and constitutes a worldwide health threat (*1*). Like other small DNA tumor viruses (i.e., SV40 and adenovirus), its genome codes for transforming oncoproteins that are essential for forcing infected cells to enter into the S phase, required for viral genome replication. It has been widely described that two HPV coded proteins, E7 and E6, are responsible for transformation and immortalization of infected cells (*2*).

The E7 oncoprotein, whose counterparts are large T antigen in SV40 and E1A in adenovirus, is the main transforming protein in HPV which promotes proteasome degradation of the cell cycle regulator retinoblastoma (*3*). On the other hand, HPV E6 oncoprotein induces the proteasome-mediated degradation of the p53 tumor suppressor protein, contributing to the oncogenic potential of HPV (*4*). It was also shown that, in addition to p53, E6 binds to a large number of cellular proteins, including transcription factors, signal transducers, proapoptotic proteins, DNA replication and repair factors, and proteins involved in cell architecture, polarity, and adhesion. Many of these proteins contain PDZ domains, such as DLG and MAG1 (*5*).

HPV E6 is a small protein of 150 amino acids, which is highly conserved among all papillomaviruses, with the most conserved regions involving two Zn binding motifs (*6*). Each Zn binding site in E6 shares the $CXXCX_{29}CXXC$ arrangement with the E7 protein (*7*). This arrangement is unique among the CCCC zinc fingers, in which usually fewer than 20 amino acids separate the cysteine pair residues (*8*). Previous biophysical characterization of recombinant HPV16 E6 suggested that the minimal functional domain sufficient for promoting *in vitro* p53 degradation comprised amino acids 2−142 of the full-length E6 protein, which contains two functionally critical zinc-bound atoms (*9*). E6 was shown to contain two stable folded domains, the E6 N- and C-terminal domains, each one of about 75 residues and with one zinc binding site (*9*, *10*). The NMR structure of the C-terminal domain of a Cys mutated form of E6 showed a novel α/*β* zinc binding fold; the N-terminal domain was proposed to share that topology based on the sequence similarity between the two domains, most likely arising from gene duplication (*7*, *11*). Soluble

†G.P.-G. and L.G.A. are Career Investigators from CONICET. A.H. holds a doctoral fellowship from CONICET.

*Corresponding author. E-mail: gpg@leloir.org.ar. Phone: +54 11 5238 7500 ext 3209. Fax: +54 11 5238 7501.

[1]Abbreviations: HPV, human papillomavirus; DTT, dithiothreitol; EDTA, *N*,*N*,*N*′,*N*′-ethylenediaminetetraacetic acid; GdmCl, guanidinium chloride; RP-HPLC, reverse-phase high-performance liquid chromatography; MALDI-TOF, matrix-assisted laser desorption ionization time of flight; CD, circular dichroism; TCEP, tris(2-carboxyethyl)phospine; AFM, atomic force microscopy; SEC, size exclusion chromatography; Tris, tris(hydroxymethyl)aminomethane; HCCA, α-cyanohydroxycinnamic acid; TFA, trifluoroacetic acid; PAR, 4-(2-pyridylazo)resorcinol; PMPS, *p*-hydroxymercuriphenylsulfonate; ThT, thioflavin T.

 Published on Web 01/12/2011

GB1 fusions of the two E6 domains were expressed, purified, and separately characterized with the tag, and higher zinc binding affinity was suggested for the C-terminal domain (*12*).

Unfused high-risk HPV E6 proteins expressed in bacteria as inclusion bodies were shown to readily assemble into large soluble oligomers of ~1.2 MDa (*13*). These oligomers are thermostable, display cooperative unfolding of secondary and tertiary structure, but have no p53 degradation promoting activity *in vitro*. Monomeric "wild-type" HPV16 and HPV18 E6 proteins are metastable in solution and slowly progress to oligomeric forms. Endogenous monomeric species were found to localize in the nucleus of transformed cell lines in agreement with its p53 degradation promoting activity, while oligomeric forms localize in the cytosol (*13*). The latter species could, on the other hand, induce proteasome degradation of PDZ-domain containing proteins, key E6 targets that are actively degraded in cytosol (*13*, *14*). The oligomerization of tagged E6 proteins from different human and bovine strains was also shown to occur in transfected cells, and self-association into insoluble ribbon-like multimers was observed *in vitro* (*15*).

In addition to the bicistronic E6/E7 transcript, alternatively spliced mRNAs code for multiple truncated species termed E6*, where the E6 ORF is modified while the E7 protein remains unchanged. In fact, these alternatively spliced forms are the most populated species in cervical tumors and in tumor-derived cell lines and appear to be present only in high-risk HPVs, not in low-risk HPV6 and HPV11 proteins due to the absence of the consensus splicing site (*16*, *17*). The E6* product of HPV18 (6.5 kDa) was detected in HPV transformed HeLa cells established in nude mice (*18*). This same species was shown to inhibit the E6-mediated degradation of p53, being the first indication of a possible regulatory role (*19*) that operates in a cell cycle dependent manner (*20*). Using a splice donor mutant of HPV16 E6, E6* was found to be preferentially localized in the cytosol (*21*). Recent studies indicated that the full-length form of HPV16 E6 accelerated the degradation of procaspase 8 DED, while E6* displayed the opposite effect (*22*); the two isoforms bind to different regions of the target protein (*23*).

Because of its small size and difficulty to form a compactly folded unit, a detailed structure was not reported to date. However, any structural and biochemical information of E6* would help to understand its biological role. Therefore, in this work we sought to characterize the conformational tendencies of the HPV16 E6* 50 aa polypeptide in solution by spectroscopic, biophysical, and chemical methods. Our results presented here indicate a "chameleon" nature of E6*, which allows this polypeptide to form different low molecular mass and oligomeric species. These conformational transitions depend on pH, redox state, metal availability, and protein levels and provide a basis for a promiscuous binding affinity. These equilibria extend to include oligomerization, the determinant of which appears to be within the E6* sequence information.

MATERIALS AND METHODS

Materials and Sample Preparation. The E6* peptide was obtained from the Keck facility (Yale University, New Haven, CT). The raw synthetic peptide, as received from the synthesis facility, was a mixture of reduced and oxidized species. To obtain a homogeneous fully reduced peptide stock, the peptide was dissolved in a solution containing 6.0 M GdmCl (Invitrogen), 50 mM DTT (Sigma Aldrich), and 5.0 mM EDTA and incubated for 24 h at 25 °C. Reduced peptide was purified by reverse-phase HPLC (RP-HPLC) in a C18 column (Thermo Scientific), lyophilized, and redissolved in 6.0 M GdmCl and 8.0 mM HCl to avoid cysteine oxidation. Unless indicated otherwise, this stock solution contains 0.5 mM reduced peptide. The molecular mass was confirmed by MALDI-TOF analysis (Bruker Microflex; Bruker Daltonics, Billerica, MA, USA). Peptide concentration of each stock solution was determined spectrophotometrically using tyrosine absorbance in 0.1 M NaOH solution at 293 nm and a molar extinction coefficient of 2400 M^{-1} cm^{-1} per tyrosine.

Circular Dichroism. All circular dichroism (CD) measurements were carried out on a Jasco J-810 spectropolarimeter (Jasco, Japan). Far-UV spectra were collected using a Peltier temperature-controlled sample holder at 20 °C and a 0.1 cm path length cell. All spectra were an average of at least 10 scans. In order to obtain soluble E6* at different pHs, a reduced peptide stock was diluted to 25 μM and dialyzed overnight at 4 °C against 50 mM sodium acetate buffer, pH 5.0, or 50 mM Tris-HCl buffer, pH 7.5. Tween 20 (0.04%) was added only to the sample at pH 7.5 to avoid extensive aggregation. In both cases TCEP at 3.0 mM final concentration was added to prevent oxidation. Zinc was added to a final concentration of 40 μM.

Atomic Force Microscopy (*AFM*). For AFM imaging, the E6* peptide was diluted to 1.0 ng/μL in buffer containing 10 mM sodium acetate, pH 5.0, and 1.0 mM TCEP. Twenty microliters of the sample was deposited onto freshly cleaved mica. After 2−5 min, the sample was gently washed with 0.5 mL of Milli-Q water to remove molecules that were not firmly attached to the mica and blow-dried with nitrogen. Tappingmode AFM was performed using a Nanoscope III Multimode atomic force microscope (Digital Instruments, Veeco Metrology, Santa Barbara, CA) using a J-type piezoelectric scanner with a maximal lateral range of 120 μm. Microfabricated silicon cantilevers 125 μm in length with a force constant of 40 N/m were used (NanoDevices, Veeco Metrology). The images (512 pixels) were captured with a scan size between 0.5 and 3.0 μm at a scan rate of 1−2 scan lines/s. Images were processed by flattering using Nanoscope software (Digital Instruments), which was used to remove background noise. WsxM 4.0 Beta 2.1 software was used to analyze the images.

Thioflavin T Fluorescence. Measurements were performed at a final peptide concentration of 10 μM in 20 mM sodium phosphate buffer at pH 7.0 and 20 μM thioflavin. The samples at different pHs were diluted at this condition to measure the emission spectra of ThT, since this reagent does not react at low pH. Emission spectra were recorded on an Aminco-Bowman spectrofluorometer at excitation and emission wavelengths of 435 and 490 nm, respectively. E7SOs oligomers (*24*) were used as a positive control.

Size Exclusion Chromatography. Analytical size exclusion chromatography (SEC) experiments for E6* were carried out on a Superdex 75 column (Amersham Pharmacia) equilibrated in 50 mM Tris-HCl buffer at pH 7.5 and 0.2 M GdmCl. Samples obtained at pH 7.5 for CD experiments were injected onto the column. The elution of the peptide was detected at 220 nm. The column was calibrated with the following standard proteins: γ-globulin (158 kDa), ovalbumin (43 kDa), myoglobin (17 kDa), and vitamin B_{12} (1.35 kDa) from a gel calibration kit (Bio-Rad).

Reverse-Phase HPLC. All RP-HPLC runs were carried out on an analytical reverse-phase C18 column using a linear gradient of 0−100% acetonitrile/H_2O containing 0.1% trifluoroacetic acid over a time period of 60 min. The eluted peptides were

detected by 220 nm absorbance. The reduced E6* sample was obtained by 10-fold dilution of a GdmCl reduced stock solution (see above, sample preparation) against 50 mM Tris-HCl buffer, pH 7.5, plus 3.0−5.0 mM freshly prepared TCEP. To obtain the homogeneous oxidized E6* species, the same procedure was performed but omitting TCEP and incubating at room temperature for 24 h. Generally, up to 15 μg of peptide was injected. The experiments were carried out at 0.6 M GdmCl residual concentration to avoid fast aggregation after diluting the stock peptide. Time course oxidation experiments were performed by diluting aliquots of reduced stock peptide in 50 mM Tris-HCl buffer, pH 7.5, alone, with 3.0−5.0 mM TCEP or 50 μM zinc as indicated. The oxidation was stopped by the addition of 0.1% TFA and analyzed by RP-HPLC as described.

MALDI-TOF Mass Spectrometry Analysis of Disulfide Bond Formation. All mass spectrometric measurements were performed on a Bruker Microflex instrument (Bruker Daltonics, Billerica, MA, USA). The samples (10 μM concentration) were mixed with an equal volume of α-cyanohydroxycinnamic acid (HCCA) dissolved in 30% acetonitrile (v/v) and 0.1% TFA (v/v), and a 2 μL aliquot was analyzed by MALDI-TOF mass spectrometry. Iodoacetamide treatment was performed by incubating either reduced or oxidized E6* peptide with 56 mM iodoacetamide in 50 mM ammonium carbonate buffer, pH 7.8, for 1 h at room temperature in the dark. All samples were precipitated and resuspended in order to eliminate iodoacetamide excess before MALDI-TOF analysis. Protein digestion was performed by adding the endoproteinase GluC at 1:25 (w/w) enzyme:peptide ratio and incubated at 25 °C for 2 h. The resulting peptides were loaded on a Zip-TipC18 (Millipore Corp., Billerica, MA) for desalting and eluted with acetonitrile/TFA, 50%/0.1%. Fragments in the mass range of 1000−4000 were selected and analyzed.

E6 Redox Potential Determination*. The redox equilibrium constant (K_{eq}) for the E6* peptide was obtained by incubating with a reference redox couple (DTT_{red}/DTT_{ox}). Briefly, 15 μg of reduced peptide was incubated for 3 h at 25 °C in 50 mM Tris-HCl buffer, pH 7.5, containing 10 mM DTT of the redox couple. Redox potential was regulated by varying DTT_{red} from 0.01 to 9.76 mM and DTT_{ox} from 0.240 to 9.99 mM while maintaining DTT final concentration fixed at 10 mM. The experiment was performed in 6 M GdmCl. Reactions were acidified by the addition of 0.1% TFA and subjected to RP-HPLC. The fraction of E6* peptide in the reduced form was calculated as the area under the curve of the HPLC peak. Data were evaluated according to eq 1:

$$R = ([DTT_{red}]/[DTT_{ox}])/(K_{eq} + [DTT_{red}]/[DTT_{ox}]) \quad (1)$$

where R is the fraction of reduced protein at equilibrium and K_{eq} is the equilibrium constant. The standard redox potential (E_0') of E6* was calculated via the Nernst equation (eq 2):

$$E_{0'\text{protein}} = E_{0'\text{reference}} - (RT/2F) \ln K_{eq} \quad (2)$$

using a value of −0.307 V for the redox potential of DTT_{red}/DTT_{ox} (*25*).

Zn Binding Experiments. Peptide concentration to be used in the assays was determined by Bradford colorimetric assay and by tyrosinate absorption at basic pH (see above, sample preparation). Bound zinc was determined by spectrophotometric measurement of the metallochromic indicator 4-(2-pyridylazo)resorcinol (PAR) (*26*). In brief, reduced purified synthetic peptide was diluted 10-fold in buffer containing reductant and zinc and incubated during 1 h at room temperature, treated with Chelex 100 (Bio-Rad) to remove soft bound metal, and purified in a PD-10 column (GE Healthcare). A 6 μM solution of this sample was incubated with 100 μM PAR and 100 μM *p*-hydroxymercuriphenylsulfonate (PMPS) in 50 mM Tris-HCl buffer, pH 7.5, and 0.2 M GdmCl. The reaction was followed at 500 nm and the amount of zinc quantified against a standard solution curve (Sigma, St. Louis, MO). The competition assay was performed by adding reduced E6* peptide to obtain 6 μM final concentration to a solution containing 6 μM zinc and 100 μM PAR in 50 mM Tirs-HCl buffer, pH 7.5, 0.6 M GdmCl, and 2.0 mM TCEP. The time trace of the $Zn(PAR)_2$ complex formation was obtained by recording absorbance at 500 nm. When indicated, PMPS and DTT were added to a final concentration of 160 and 250 μM, respectively. For zinc titration experiments, a solution containing 100 μM PAR and 6 μM E6* in 50 mM Tris-HCl buffer, pH 7.5, 0.6 M GdmCl, and 2.0 mM TCEP was titrated by the addition of 2.5 μL of concentrated $ZnSO_4$ stock solution. Absorbance at 500 nm was measured, and the titration point was obtained graphically.

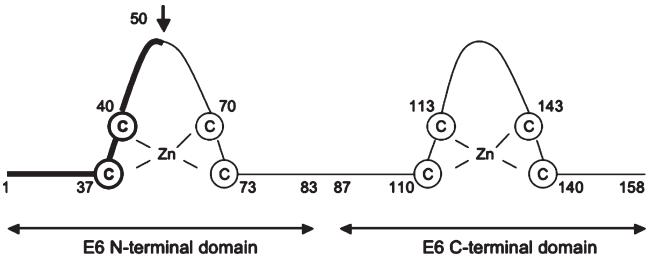

FIGURE 1: Schematic representation of the HPV16 E6 sequence. E6* encompasses residues 1−50 of the full-length E6 protein, which are highlighted in bold line. The black arrow indicates a splice donor site, only present in high-risk HPV E6 proteins. The amino acid positions of cysteine residues involved in zinc coordination are shown. The E6* polypeptide conserves only half of the N-terminal zinc binding motif (Cys 37 and Cys 40).

RESULTS

Folding of E6 in Solution*. Our first goal was to study conditions in which E6* attained a stable conformation in solution. For this purpose, we use a peptide comprising amino acids 1−50 of E6, assuming the first putative methionine residue as the translation start site (*27*), and contains half of the N-terminal zinc binding motif of E6 (Figure 1). Preliminary experiments indicated that E6* was rather insoluble and required high GdmCl concentrations and a reductant for solubilization of the synthetic peptide. The GdmCl solubilized E6* peptide was initially diluted into aqueous buffer at pH 5.0, resulting in a soluble species with a high β-sheet content, as judged by its far-UV CD spectrum, which presented a CD minimum at 217 nm (Figure 2A). Given the small size of the truncated polypeptide and the occurrence of this type of secondary structure in proteins that are prone to assemble into high molecular mass oligomers, we decided to evaluate the presence of oligomeric structures. Dynamic light scattering measurements showed species of ∼32 nm diameter (data not shown) equivalent to a 2.2 MDa globular protein, clearly indicating that the peptide oligomerized. However, we cannot rule out the existence of heterogeneities. When inspected under the atomic force microscope, two main populations of oligomers became evident (Figure 2C,D). Worm-like structures coexisted with smaller spherical structures of around 5 nm (Figure 2C,D). The β-sheet structure observed remained

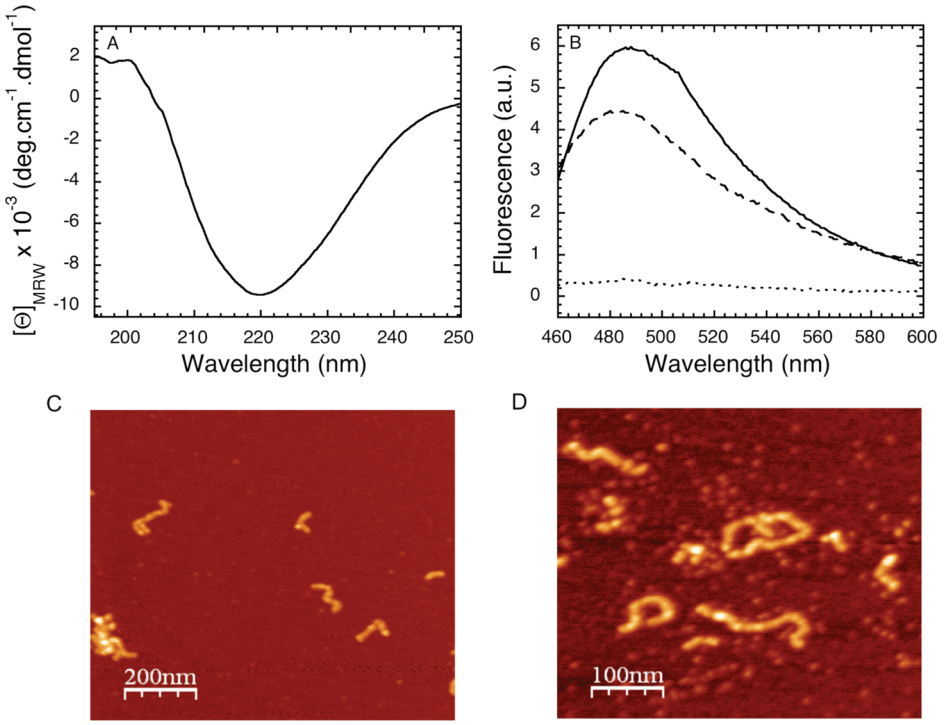

FIGURE 2: E6* conformational behavior at pH 5.0. (A) Far-UV CD spectrum of E6* in 50 mM acetate buffer, pH 5.0. (B) Thioflavin T fluorescence spectra of E6*, pH 7.5 (···), E6*, pH 5.0 (- - -), and E7SOs (—) as a positive control. The contribution of free ThT at each pH was subtracted. (C, D) Visualization of E6* β-sheet oligomer in 50 mM acetate buffer, pH 5.0, by AFM. (C) The *xy* scale corresponds to 1 μm. (D) The *xy* scale corresponds to 0.5 μm.

stable in solution and stood several freeze−thaw cycles. Given the oligomeric and fiber-like structure of the components, we tested for thioflavin T binding that would indicate oligomeric repetitive β-sheet structure (*28*). The emission fluorescence spectrum of the dye incubated with oligomeric E6* obtained at acidic pH showed an increased intensity when compared to the dye alone. This spectrum was similar to the one obtained for the HPV E7 β-sheet-rich oligomers (E7SOs), used as a positive control (*24*) (Figure 2B).

On the other hand, at pH 7.5, E6* refolds into oligomeric species enriched in α-helical secondary structure, as indicated by its far-UV CD spectrum, with two minima around 208 and 222 nm and a positive band at 198 nm (Figure 3A). Unlike the β-sheet oligomeric species obtained at pH 5.0, these oligomers tended to aggregate and could only remain in solution for a few hours. This feature prevented a more extensive characterization of this species. As opposed to the β-sheet oligomeric species, the E6* α-oligomer did not bind ThT (Figure 2B).

Due to the relevance of zinc in the overall folding of the full-length E6 protein, we decided to assess the effect of this metal on E6* conformation. When zinc was added into the refolding buffer at pH 7.5, we obtained a stable and soluble species with a CD spectrum characteristic of a more disordered structure but with unequivocal indication of residual secondary structure content (Figure 3A). A negative shoulder at 228 nm and a positive one at around 215 nm suggested the combination of two different and mixed contributions. In addition, the minimum at 198 nm, typical of coil conformation, was shifted to 203 nm. When the α-oligomers were subjected to size exclusion chromatography right after refolding in the absence of zinc, the sample eluted at the void volume (> 70 kDa), confirming an oligomeric nature (Figure 3B).

A different hydrodynamic behavior was observed when the E6* peptide was refolded in the presence of zinc. The zinc-containing

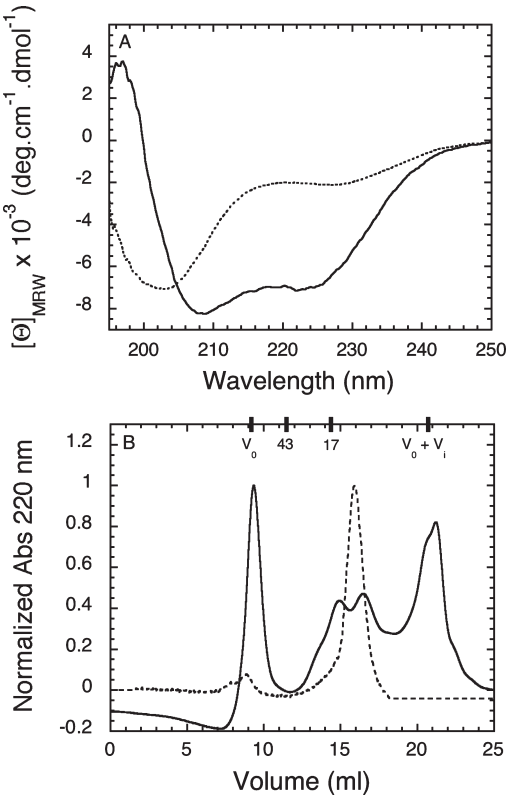

FIGURE 3: E6* conformational behavior at pH 7.5. (A) Far-UV CD spectra of E6* in 50 mM Tris-HCl buffer, pH 7.5 (—), and with the addition of 40 μM zinc (···). (B) Size exclusion chromatography of E6* in Tris-HCl buffer, pH 7.5, alone (—) and in the presence of zinc (···). Elution volumes for globular molecular mass markers (in kDa), V_0 and $V_0 + V_i$ are indicated with bars. All samples contain TCEP as reductant.

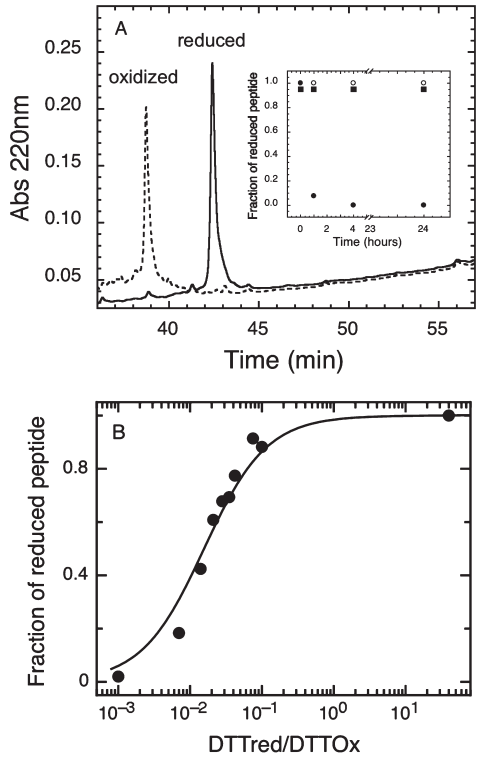

FIGURE 4: E6* redox state analyzed by RP-HPLC. (A) RP-HPLC chromatograms of oxidized (···) and reduced (—) E6* in 50 mM Tris-HCl buffer, pH 7.5, 0.6 M GdmCl (see Materials and Methods). Inset: Oxidation kinetics of E6* in the absence (●) or presence (○) of TCEP as reductant and in the presence of zinc (■), analyzed by RP-HPLC. The amounts of reduced forms were obtained from the integration of peak areas from the chromatograms. (B) Redox equilibrium of E6* with DTT. Fractions of reduced E6* obtained after incubation with variable ratios of the redox couple DTT_{red}/DTT_{ox} were plotted against DTT_{red}/DTT_{ox}. The data were analyzed as described in Materials and Methods. The equilibrium constant (K_{eq}) and the standard redox potential of E6*, at 25 °C, pH 7.5, and 6.0 M GdmCl, were determined to be 0.016 and −0.254 V, respectively.

species eluted as an ~9 kDa globular protein (Figure 3B), which did not allow for discrimination between monomeric and dimeric E6* species. The high symmetry and lack of significant oligomeric species strongly suggested that the metal was preventing or disrupting the oligomerization. Addition of zinc had no effect on the formation or stability of the β-sheet oligomeric species at pH 5.0 (Figure S1, Supporting Information).

Redox State of Conserved E6 Cysteine Residues*. Preliminary experiments showed a marked tendency of E6* to aggregate in the absence of metal or reductant. Since this peptide contains three highly conserved cysteine residues, we decided to analyze the possible oxidation of these residues and the redox state of the formed species. Our first approach was to measure the time course of the spontaneous oxidation of the E6* peptide in Tris-HCl buffer at pH 7.5. Briefly, an aliquot of fully reduced unfolded peptide was diluted in neutral buffer, in either the presence or absence of reductant or zinc, and was let air-oxidize. At different time points aliquots were withdrawn and subjected to RP-HPLC to separate and quantify the reduced and oxidized E6* species. It should be mentioned that, in order to fully reduce the stock peptide, concentrations of over 50 mM DTT and high denaturant concentration were required (see Materials and Methods). In order to avoid fast aggregation when diluting the stock peptide, the experiments were performed at a residual 0.6 M GdmCl concentration. Spontaneous air oxidation occurred within the first hour (Figure 4A); however, the addition of zinc prevented this oxidation, suggesting that at least one of the cysteine side chains of the half-zinc binding motif was oxidized. Interestingly, zinc precluded the oxidation of the peptide to the same extent as 5.0 mM TCEP, a potent reductant. This observation strongly suggested that the E6* peptide, containing only half of the canonical zinc binding motif present in full-length E6 protein, could coordinate the metal with an affinity that was strong enough to prevent the redox reactivity of cysteine residues.

Mass spectral analysis indicated that oxidized E6* treated with iodoacetamide had only one free reactive cysteine. Fully reduced and carboxymethylated E6* peptide exhibited three reactive cysteine residues, as expected from the sequence (Figure S2, Supporting Information). As only the monomeric E6* form was observed in the oxidized sample, we inferred that the other two nonreactive cysteine residues were involved in an intramolecular disulfide bridge (Figure S2, Supporting Information). MALDI-TOF analysis of the fragments obtained by enzymatic digestion of oxidized E6* confirmed that the neighboring cysteines (Cys 37 and Cys 40), corresponding to the half-zinc binding motif, were linked by a disulfide bridge (Table 1, Supporting Information).

Finally, we aimed at determining the redox potential of the formed disulfide bridge. Since the oxidized species had a strong tendency for aggregation, we carried out the experiments in 6 M GdmCl. The peptide was incubated with variable ratios of the redox couple DTT_{red}/DTT_{ox}, and the peak area obtained from the RP-HPLC chromatogram was used to determine the reduced/oxidized peptide fractions (Figure 4B). A K_{ox} of 0.016 was obtained, corresponding to a redox potential of −254 mV.

E6 Zn Binding Properties*. In order to determine the stoichiometry and affinity of the zinc bound to E6*, we performed a colorimetric quantification of the bound metal using the PAR-PMPS assay (*26*). First, the E6*:Zn stoichiometry was estimated by quantifying the amount of zinc that remained strongly bound to the E6* peptide after refolding in the presence of the metal. A stoichiometry of 2 mol of peptide/mol of zinc was obtained, suggesting a 2:1 complex.

Next, we determined the apparent affinity of the E6*−Zn complex by dissociating the $Zn(PAR)_2$ complex with reduced E6* peptide. When a stoichiometric amount of E6* (1 μmol of E6*/μmol of zinc) was added to a $Zn(PAR)_2$ solution, only 50% of the metal was displaced within seconds (Figure 5A). Considering the previously reported K_D of 10^{-12} M for the $Zn(PAR)_2$ complex (*26*), our results indicate that the affinity of the E6*−Zn interaction is much higher than that of the $Zn(PAR)_2$ complex ($K_D \ll 10^{-12}$ M), especially if we consider the fast kinetics involved. The 50% displacement also indicates a 2:1 E6*:Zn stoichiometry, strongly suggesting an E6* dimer linked by the metal. The addition of the organomercurial thiol reactive reagent PMPS completely dissociated the E6*−Zn complex as expected for a sulfur-coordinating ligand, further confirming the involvement of a cysteine residue in zinc binding (Figure 5A). In the presence of a large excess of DTT, the PMPS was detached from the cysteines, and the zinc was readily rebound by the peptide, indicating a fully reversible reaction (Figure 5A). Moreover, as the reversibility was measured in the presence of PAR, this result further supports the high-affinity constant for the E6*−Zn complex.

Finally, we aimed to determine the stoichiometry of the E6*−Zn complex by titrating a fixed concentration of reduced E6* peptide in the presence of PAR with increasing amounts of zinc. As the apparent affinity constant for the E6*I−Zn complex is expected to

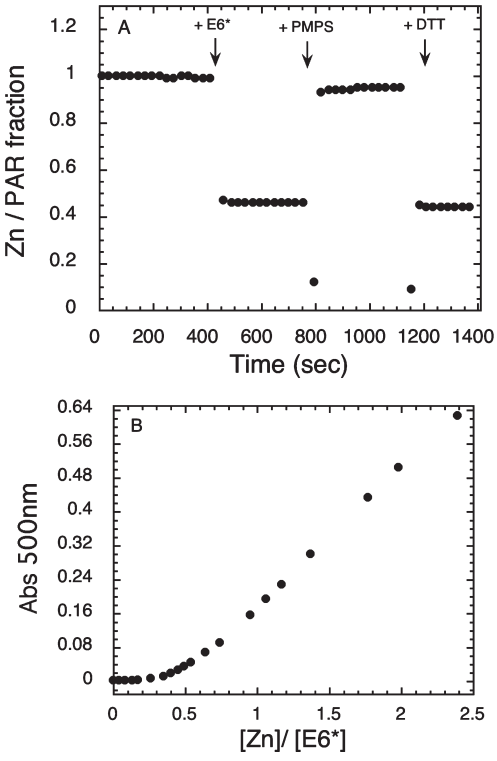

FIGURE 5: E6* zinc binding properties. (A) Competition assay. Absorbance of the $Zn(PAR)_2$ complex was monitored at 500 nm over time after the addition of stoichiometric amounts of E6* (1 μmol of E6*/μmol of zinc). Absorbance was measured during 5 min before addition of 160 μM PMPS and finally 250 μM DTT. (B) Zinc titration of E6*. Titration of 100 μM PAR and 6 μM E6* polypeptide with increasing concentrations of zinc. Absorbance at 500 nm, indicative of formation of the $Zn(PAR)_2$ complex, was plotted as a function of the [Zn]/[E6*] monomer ratio.

be higher than the one for the $Zn(PAR)_2$ complex, the point at which the absorbance at 500 nm starts to increase indicates the saturation of the E6* binding site. Careful addition of zinc to a solution of E6* in the presence of PAR showed titration at a 0.5:1 Zn:E6* ratio, confirming the stoichiometry obtained previously (Figure 5B).

DISCUSSION

Transcription of most known HPV genes in the context of the full genome, either in early or late stages of the virus life cycle, leads to a plethora of alternatively spliced and chimeric products. However, it is difficult to detect protein levels at the early stages of natural infection, including those of chimeric nature. Moreover, the splicing patterns greatly vary depending on the cell line, either in naturally transformed or in transfected cells (*29*−*33*). Arguably, the most abundantly spliced product in high-risk HPV transformed cell lines is the one that leads to breaking the E6 coding frame and yields E6*, produced at even higher levels than full-length E6. One intriguing aspect is that this splice site is conserved only in high-risk strains (*16*, *17*, *34*).

There are only a few reports of the detection of E6* by Western blot in HPV-transformed or transfected cells, and antibodies that can discriminate both species are not yet available; thus, studies are mostly focused on RNA transcripts. Such a conserved splicing site, despite having an enhancing effect on transcription of the downstream E7 oncogene (*34*, *35*), must necessarily produce significant amounts of the E6* polypeptide. Although different functional roles were assigned to E6* (*22*, *36*−*38*), there is no structural characterization of this 50 aa polypeptide. In this work, we set out to investigate the conformational tendencies of the 50mer HPV16 E6* polypeptide product in solution, as we deemed it necessary for understanding its functional role in the presence or absence of E6.

E6*, as it came from synthesis, was solubilized in GdmCl and DTT. Once solubilized at pH 5.0, the peptide refolds into a highly stable β-sheet oligomer, irrespective of whether zinc is present or not. As we previously described, "wild-type" HPV16 and HPV18 E6 self-assemble into large oligomers in the absence of zinc. In addition, endogenous oligomeric forms were found in HPV naturally transformed CaSki and HeLa cell lines, preferentially localized in the cytosol, as opposed to monomeric E6, present in the nucleus (*13*). Unlike the full-length E6 oligomers we described previously (*13*), the soluble E6* oligomers bind thioflavin T, which is a characteristic of repetitive β-sheet structure (*28*). Although we are not able to explain at this stage the structural basis for this difference, E6* has a strong tendency to oligomerize in aqueous solution, suggesting that it is responsible for the oligomerization of full-length E6.

At pH 7.5, E6* also oligomerizes but to a α-helical containing structure, with no affinity for thioflavin T and a tendency to slowly progress into insoluble aggregates. However, opposite to the stable β-sheet oligomers obtained at pH 5.0, the presence of zinc completely prevents the formation of these α-helical oligomers, leading to a low molecular mass species lacking canonical secondary structure but with a far-UV CD spectrum indicative of significant structure (Figure 3A). In an intracellular context, the equilibrium between oligomeric versus low molecular mass species will be dictated by the availability of zinc (*39*). In addition, a redox contribution is also expected, and E6* readily oxidizes to a species containing a disulfide bond between neighboring cysteine residues (37 and 40), with a redox potential of −0.254 V in the range of well-described redox proteins such as thioredoxin (*40*). This disulfide bond is not formed if zinc is present, which strongly suggests that the high affinity for zinc is required and opposes to the formation of a local disulfide. In addition, amyloid oligomerization was shown to be specifically modulated by zinc in model peptides (*41*).

The affinity of E6* for zinc is higher than that of PAR ($K_D < 10^{-12}$ M) (*26*), and the E6*−Zn complex is formed almost instantly, further supporting a very high affinity. Titration experiments clearly show a 2:1 E6*:Zn ratio, implying that this high affinity is based on the formation of a zinc-bound E6* dimer. Under these conditions, E6* remains in solution without forming oligomers or aggregates, and a tetrahedral coordination could explain this unusually high affinity. It should be mentioned that, although the actual value of the zinc coordination affinity constant has not been determined, this apparent constant is in the order of other well-documented Zn binding proteins that are physiologically regulated by its zinc content (*42*), suggesting that metal can regulate E6* conformation or function in the cell. In the context of a nascent E6* polypeptide and in the absence of the rest of the E6 sequence, E6* is unlikely to adopt a native conformation, that is, the one adopted by the full-length E6. The fate of this species will be linked to a balance between zinc availability and redox potential combined with oligomerization. In the absence of available zinc, or in a large excess of E6*, which is a plausible scenario, the oligomeric species would be the more stable. Since our previous results on the cytosolic localization of E6 oligomers were not based on E6*-specific antibodies (*13*), we cannot discriminate among species, but we suspect that, given the excess of E6* transcripts in HPV-transformed cell lines (i.e., after

genome integration), this small polypeptide product could be a considerable component if not the most abundant species, either as a homo- or as a heterooligomer (*21*, *43*). Furthermore, all evidence presented in this work indicates that the oligomerization determinant is present within E6*.

We hypothesize that oligomerization equilibria within cells are directly linked to E6*/E6 absolute individual or relative levels. This ratio was shown to fluctuate along cell cycle progression (*20*), resulting in different effects depending on the relative amounts of the different species (*43*). In addition, it was shown that the spliced product containing E6* is required for optimal transcription of the downstream E7 gene (*34*, *35*); this event was shown to be modulated by EGF, implying that the relative levels also change across the different layers of the infected epithelium (*44*). Moreover, high levels of E7 transcripts require low levels of E6, at the expense of E6* products. Although not yet demonstrated, this is likely reflected in the polypeptide products. Therefore, high levels of E7 protein (progression to S phase via Rb degradation) imply low levels of E6 (avoiding the checkpoint by p53 degradation) through increased levels of E6*. High levels of E6* polypeptide counteract E6 action, thus, ensuring progression to S phase for viral DNA synthesis under p53 control.

Overall, the characterization of E6* presented in this work contributes to the understanding of its mechanism of action. We show that E6* can form low molecular mass species with residual but significant structure that can oligomerize to different conformations depending on the chemical environment, zinc availability, and redox state. We propose that its marked conformational plasticity is the basis for the wide range of E6 protein interactions, by its capacity to accommodate to binding sites of different nature. On the basis of our results, we infer that E6* is unlikely to be homogeneous and stable as an isolated protein; in contrast, E6* was hypothesized to form a heterodimer with E6, but this is yet to be demonstrated. Instead, we believe that E6* is more likely to cooligomerize to high molecular structures with E6, but also with many of the other cellular targets described. This would particularly take place when the protein levels are high, exceed the available zinc, and favor oligomerization.

Although E6 is not an intrinsically disordered protein like E7 (*45*, *46*), both proteins oligomerize in the absence of zinc or, in other words, when the protein levels exceed those of free zinc in the cytosol. Similar to the case of E7-Rb, p53 could be the primary target of E6 in early infection when the oncoprotein levels are low. Upon loss of E2 repression after viral genome integration, both E6 and E6* species may shoot up and start affecting many of the other targets described. It should be pointed out that no structural−biochemical mechanistic description of E6−p53 interaction (whether directly or mediated by E6AP) and no quantitative information on the relative affinities for p53 with respect to other target are available. Future studies addressing the actual levels of the E6*/E6 proteins in cellular models, as well as the subcellular localization of both species, will be highly relevant. The functional significance of this alternative splicing site present only in E6 proteins derived from high-risk strains or its existence as a collateral product of regulatory splicing stands as a fundamental question in HPV biology and cancer progression.

ACKNOWLEDGMENT

We thank Lucia Beatriz Chemes for helpful criticisms to the manuscript and Diana E. Wetzler for her contribution in early discussions.

SUPPORTING INFORMATION AVAILABLE

Two figures and one table including far-UV CD spectra of E6* at pH 5.0 with and without zinc, MALDI-TOF spectra of reduced and oxidized E6* species, schematic representation of the disulfide bridge formed, and a table with data of enzymatic digestion of reduced and oxidized E6* species. This material is available free of charge via the Internet at http://pubs.acs.org.

REFERENCES

1. zur Hausen, H. (1996) Papillomavirus infecions: a major cause of human cancers. *Biochim. Biophys. Acta 1288*, 55–78.
2. Munger, K., Phelps, W. C., Bubb, V., Howley, P. M., and Schlegel, R. (1989) The E6 and E7 genes of the human papillomavirus type 16 together are necessary and sufficient for transformation of primary human keratinocytes. *J. Virol. 63*, 4417–4421.
3. Boyer, S. N., Wazer, D. E., and Band, V. (1996) E7 protein of human papilloma virus-16 induces degradation of retinoblastoma protein through the ubiquitin-proteasome pathway. *Cancer Res. 56*, 4620–4624.
4. Scheffner, M., Werness, B. A., Huibregtse, J. M., Levine, A. J., and Howley, P. M. (1990) The E6 oncoprotein encoded by human papillomavirus types 16 and 18 promotes the degradation of p53. *Cell 63*, 1129–1136.
5. Howie, H. L., Katzenellenbogen, R. A., and Galloway, D. A. (2009) Papillomavirus E6 proteins. *Virology 384*, 324–334.
6. Ullman, C. G., Haris, P. I., Galloway, D. A., Emery, V. C., and Perkins, S. J. (1996) Predicted alpha-helix/beta-sheet secondary structures for the zinc-binding motifs of human papillomavirus E7 and E6 proteins by consensus prediction averaging and spectroscopic studies of E7. *Biochem. J. 319* (Part 1), 229–239.
7. Cole, S. T., and Danos, O. (1987) Nucleotide sequence and comparative analysis of the human papillomavirus type 18 genome. Phylogeny of papillomaviruses and repeated structure of the E6 and E7 gene products. *J. Mol. Biol. 193*, 599–608.
8. Berg, J. M., and Shi, Y. (1996) The galvanization of biology: a growing appreciation for the roles of zinc. *Science* (*New York*) *271*, 1081–1085.
9. Lipari, F., McGibbon, G. A., Wardrop, E., and Cordingley, M. G. (2001) Purification and biophysical characterization of a minimal functional domain and of an N-terminal Zn^{2+}-binding fragment from the human papillomavirus type 16 E6 protein. *Biochemistry 40*, 1196–1204.
10. Nomine, Y., Charbonnier, S., Ristriani, T., Stier, G., Masson, M., Cavusoglu, N., Van Dorsselaer, A., Weiss, E., Kieffer, B., and Trave, G. (2003) Domain substructure of HPV E6 oncoprotein: biophysical characterization of the E6 C-terminal DNA-binding domain. *Biochemistry 42*, 4909–4917.
11. Nomine, Y., Masson, M., Charbonnier, S., Zanier, K., Ristriani, T., Deryckere, F., Sibler, A. P., Desplancq, D., Atkinson, R. A., Weiss, E., Orfanoudakis, G., Kieffer, B., and Trave, G. (2006) Structural and functional analysis of E6 oncoprotein: insights in the molecular pathways of human papillomavirus-mediated pathogenesis. *Mol. Cell 21*, 665–678.
12. Liu, Y., Cherry, J. J., Dineen, J. V., Androphy, E. J., and Baleja, J. D. (2009) Determinants of stability for the E6 protein of papillomavirus type 16. *J. Mol. Biol. 386*, 1123–1137.
13. García-Alai, M. M., Dantur, K. I., Smal, C., Pietrasanta, L., and de Prat-Gay, G. (2007) High risk HPV E6 oncoproteins assemble into large oligomers that allow localization of endogenous species in prototypic HPV transformed cell lines. *Biochemistry 46*, 341–349.
14. Moody, C. A., and Laimins, L. A. (2010) Human papillomavirus oncoproteins: pathways to transformation. *Nature Rev. 10*, 550–560.
15. Zanier, K., Ruhlmann, C., Melin, F., Masson, M., Ould M'hamed Ould Sidi, A., Bernard, X., Fischer, B., Brino, L., Ristriani, T., Rybin, V., Baltzinger, M., Vande Pol, S., Hellwig, P., Schultz, P., and Trave, G. (2010) E6 proteins from diverse papillomaviruses self-associate both in vitro and in vivo. *J. Mol. Biol. 396*, 90–104.
16. Schneider-Gadicke, A., and Schwarz, E. (1986) Different human cervical carcinoma cell lines show similar transcription patterns of human papillomavirus type 18 early genes. *EMBO J. 5*, 2285–2292.
17. Smotkin, D., and Wettstein, F. O. (1986) Transcription of human papillomavirus type 16 early genes in a cervical cancer and a cancer-derived cell line and identification of the E7 protein. *Proc. Natl. Acad. Sci. U.S.A. 83*, 4680–4684.
18. Schneider-Gadicke, A., Kaul, S., Schwarz, E., Gausepohl, H., Frank, R., and Bastert, G. (1988) Identification of the human papillomavirus

type 18 E6 and E6 proteins in nuclear protein fractions from human cervical carcinoma cells grown in the nude mouse or in vitro. *Cancer Res. 48*, 2969–2974.
19. Pim, D., Massimi, P., and Banks, L. (1997) Alternatively spliced HPV-18 E6* protein inhibits E6 mediated degradation of p53 and suppresses transformed cell growth. *Oncogene 15*, 257–264.
20. Guccione, E., Pim, D., and Banks, L. (2004) HPV-18 E6*I modulates HPV-18 full-length E6 functions in a cell cycle dependent manner. *Int. J. Cancer 110*, 928–933.
21. Vaeteewoottacharn, K., Chamutpong, S., Ponglikitmongkol, M., and Angeletti, P. C. (2005) Differential localization of HPV16 E6 splice products with E6-associated protein. *Virol. J. 2*, 50.
22. Filippova, M., Johnson, M. M., Bautista, M., Filippov, V., Fodor, N., Tungteakkhun, S. S., Williams, K., and Duerksen-Hughes, P. J. (2007) The large and small isoforms of human papillomavirus type 16 E6 bind to and differentially affect procaspase 8 stability and activity. *J. Virol. 81*, 4116–4129.
23. Tungteakkhun, S. S., Filippova, M., Fodor, N., and Duerksen-Hughes, P. J. (2010) The full-length isoform of human papillomavirus 16 E6 and its splice variant E6* bind to different sites on the procaspase 8 death effector domain. *J. Virol. 84*, 1453–1463.
24. Alonso, L. G., Garcia-Alai, M. M., Smal, C., Centeno, J. M., Iacono, R., Castano, E., Gualfetti, P., and de Prat-Gay, G. (2004) The HPV16 E7 viral oncoprotein self-assembles into defined spherical oligomers. *Biochemistry 43*, 3310–3317.
25. Rozhkova, A., and Glockshuber, R. (2007) Kinetics of the intramolecular disulfide exchange between the periplasmic domains of DsbD. *J. Mol. Biol. 367*, 1162–1170.
26. Hunt, J. B., Neece, S. H., and Ginsburg, A. (1985) The use of 4-(2-pyridylazo)resorcinol in studies of zinc release from *Escherichia coli* aspartate transcarbamoylase. *Anal. Biochem. 146*, 150–157.
27. Androphy, E. J., Hubbert, N. L., Schiller, J. T., and Lowy, D. R. (1987) Identification of the HPV-16 E6 protein from transformed mouse cells and human cervical carcinoma cell lines. *EMBO J. 6*, 989–992.
28. LeVine, H., III (1999) Quantification of β-sheet amyloid fibril structures with thioflavin T. *Methods Enzymol.,* 309.
29. Grassmann, K., Rapp, B., Maschek, H., Petry, K. U., and Iftner, T. (1996) Identification of a differentiation-inducible promoter in the E7 open reading frame of human papillomavirus type 16 (HPV-16) in raft cultures of a new cell line containing high copy numbers of episomal HPV-16 DNA. *J. Virol. 70*, 2339–2349.
30. Milligan, S. G., Veerapraditsin, T., Ahamet, B., Mole, S., and Graham, S. V. (2007) Analysis of novel human papillomavirus type 16 late mRNAs in differentiated W12 cervical epithelial cells. *Virology 360*, 172–181.
31. Ozbun, M. A., and Meyers, C. (1997) Characterization of late gene transcripts expressed during vegetative replication of human papillomavirus type 31b. *J. Virol. 71*, 5161–5172.
32. Ordonez, R. M., Espinosa, A. M., Sanchez-Gonzalez, D. J., Armendariz-Borunda, J., and Berumen, J. (2004) Enhanced oncogenicity of Asian-American human papillomavirus 16 is associated with impaired E2 repression of E6/E7 oncogene transcription. *J. Gen. Virol. 85*, 1433–1444.
33. Doorbar, J., Parton, A., Hartley, K., Banks, L., Crook, T., Stanley, M., and Crawford, L. (1990) Detection of novel splicing patterns in a HPV16-containing keratinocyte cell line. *Virology 178*, 254–262.
34. Tang, S., Tao, M., McCoy, J. P., Jr., and Zheng, Z. M. (2006) The E7 oncoprotein is translated from spliced E6*I transcripts in high-risk human papillomavirus type 16- or type 18-positive cervical cancer cell lines via translation reinitiation. *J. Virol. 80*, 4249–4263.
35. Del Moral-Hernandez, O., Lopez-Urrutia, E., Bonilla-Moreno, R., Martinez-Salazar, M., Arechaga-Ocampo, E., Berumen, J., and Villegas-Sepulveda, N. (2010) The HPV-16 E7 oncoprotein is expressed mainly from the unspliced E6/E7 transcript in cervical carcinoma C33-A cells, *Arch. Virol. 155*, 1959−1970
36. Pim, D., Tomaic, V., and Banks, L. (2009) The human papillomavirus (HPV) E6* proteins from high-risk, mucosal HPVs can direct degradation of cellular proteins in the absence of full-length E6 protein. *J. Virol. 83*, 9863–9874.
37. Pim, D., and Banks, L. (1999) HPV-18 E6*I protein modulates the E6-directed degradation of p53 by binding to full-length HPV-18 E6. *Oncogene 18*, 7403–7408.
38. Storrs, C. H., and Silverstein, S. J. (2007) PATJ, a tight junction-associated PDZ protein, is a novel degradation target of high-risk human papillomavirus E6 and the alternatively spliced isoform 18 E6. *J. Virol. 81*, 4080–4090.
39. Outten, C. E., and O'Halloran, T. V. (2001) Femtomolar sensitivity of metalloregulatory proteins controlling zinc homeostasis. *Science (New York) 292*, 2488–2492.
40. Gilbert, H. F. (1995) Thiol/disulfide exchange equilibria and disulfide bond stability. *Methods Enzymol. 251*, 8–28.
41. Alies, B., Pradines, V., Llorens-Alliot, I., Sayen, S., Guillon, E., Hureau, C., and Faller, P. (2010) Zinc(II) modulates specifically amyloid formation and structure in model peptides, *J. Biol. Inorg. Chem.* (in press).
42. Maret, W. (2004) Zinc and sulfur: a critical biological partnership. *Biochemistry 43*, 3301–3309.
43. Filippova, M., Filippov, V. A., Kagoda, M., Garnett, T., Fodor, N., and Duerksen-Hughes, P. J. (2009) Complexes of human papillomavirus type 16 E6 proteins form pseudo-death-inducing signaling complex structures during tumor necrosis factor-mediated apoptosis. *J. Virol. 83*, 210–227.
44. Rosenberger, S., De-Castro Arce, J., Langbein, L., Steenbergen, R. D., and Rosl, F. (2010) Alternative splicing of human papillomavirus type-16 E6/E6* early mRNA is coupled to EGF signaling via Erk1/2 activation. *Proc. Natl. Acad. Sci. U.S.A. 107*, 7006–7011.
45. Alonso, L. G., Garcia-Alai, M. M., Nadra, A. D., Lapena, A. N., Almeida, F. L., Gualfetti, P., and de Prat-Gay, G. (2002) High-risk (HPV16) human papillomavirus E7 oncoprotein is highly stable and extended, with conformational transitions that could explain its multiple cellular binding partners. *Biochemistry 41*, 10510–10518.
46. Uversky, V. N., Roman, A., Oldfield, C. J., and Dunker, A. K. (2006) Protein intrinsic disorder and human papillomaviruses: increased amount of disorder in E6 and E7 oncoproteins from high risk HPVs. *J. Proteome Res. 5*, 1829–1842.